A method for quantifying annihilation rates of bulk point defects at surfaces

Charlotte T. M. Kwok, Kapil Dev, Richard D. Braatz, and E. G. Seebauer[a)]
Department of Chemical and Biomolecular Engineering, University of Illinois at Urbana–Champaign, Urbana, Illinois 61801-3602

(Received 10 January 2005; accepted 10 May 2005; published online 8 July 2005)

Point defects such as vacancies and interstitial atoms serve as primary mediators of solid-state diffusion in many materials. In some cases, the defects encounter surfaces where annihilation can occur. Quantification of annihilation rates presents formidable challenges, since point defect concentrations are typically low and therefore difficult to monitor directly. The present work develops a method for such quantification based upon measurements of diffusional profile spreading of a foreign species, using as an example isotopically labeled silicon implanted into a silicon matrix. Optimal experimental design techniques together with maximum-likelihood estimation indicate that the loss probability for Si interstitials on nitrogen-covered Si(100) lies at 7.1×10^{-4}. © *2005 American Institute of Physics*. [DOI: 10.1063/1.1946195]

I. INTRODUCTION

Point defects such as vacancies and interstitial atoms serve as primary mediators of solid-state diffusion in many materials. In some applications, the defects encounter surfaces (or solid interfaces) where annihilation can take place. When the physical dimensions of the solid are sufficiently small, such surfaces can become the primary means by which solids that are supersaturated with defects move toward equilibrium. Such supersaturation occurs in a wide variety of situations, e.g., during mechanical deformation or rapid quenching of hot solids, as a result of film growth due to oxidation[1,2] or nitridation,[3,4] or in response to direct atom injection from ion implantation.

The rate of equilibration is paramount in applications such as the measurement of solid-phase diffusion coefficients and the transient-enhanced diffusion of dopants after ion implantation for integrated circuit manufacture.[5] However, surface annihilation rates have never been measured. Such measurements present formidable challenges, since point defect concentrations are typically low and therefore difficult to monitor directly. It often proves easier to monitor the concentration of some species present in higher concentration that serves as a marker for the defects.

The present work demonstrates an example of how to use this latter approach by quantifying surface annihilation rates of silicon interstitials at the Si(100) surface through measurements of self-diffusion. Supersaturation is achieved through ion implantation of isotopically labeled silicon into a crystalline substrate, and the evolution of the resulting profiles upon annealing is monitored with secondary-ion-mass spectroscopy (SIMS). Optimal experimental design helps to minimize the number of experiments required and to maximize the sensitivity of the profiles to the annihilation rates. Maximum-likelihood estimation provides rigorous estimates of the annihilation rates and the associated confidence intervals.

II. EXPERIMENT

A. Laboratory procedure

Experiments were performed in a turbomolecularly pumped ultrahigh-vacuum chamber described elsewhere[6,7] with a base pressure in the low 10^{-10}-torr range. The chamber was equipped with a variable energy ion gun (up to 2.0 keV) for ion implantation, and with retarding field optics for Auger electron spectroscopy (AES). Specimens with dimensions of 1.2×1.0 cm^2 were cut from Si(100) wafers. Resistive heating was employed, with temperature monitored by a Chromel-Alumel thermocouple.

The Si(100) wafers were prepared with 0.5-μm-thick layers of isotopically labeled epitaxial Si. The layers were grown by low-pressure chemical-vapor deposition (by Isonics Corp.), and were depleted in the mass 30 isotope to 0.002% (compared to the natural abundance of 3.10%). This depletion increased the sensitivity of the experiment, since the implanted Si atoms consisted of roughly 90% mass 30. The substrate wafers were *p* type, doped with boron to a level of 1×10^{19} cm^{-3}. The grown layer was also B doped, but to a level of 10^{15} cm^{-3}.

Implantation was accomplished using SiH_4 gas that was enriched in the ^{30}Si isotope. The gas was obtained from Voltaix Corp., with impurities consisting primarily of carbon. To achieve a degree of surface passivation, specimen surfaces could be exposed to NH_3 (99.99%) before implantation. Voronkov *et al.* have shown[8] that such passivation can reduce the rate of Si interstitial annihilation at the surface. We found that such passivation increased the degree of profile spreading, and therefore the precision with which the surface annihilation rate for interstitials could be measured. Voronkov *et al.* employed oxygen for passivation, but in our ultrahigh-vacuum environment, thin oxide can desorb as SiO

[a)]Author to whom correspondence should be addressed; electronic mail: eseebaue@uiuc.edu

at high temperatures. Therefore, we employed nitrogen for passivation, since there exists no equivalent desorption pathway. Exposure to ammonia took place at 800 °C for 5 min. Under these conditions, less than one monolayer of nitrogen adsorbed on the surface, as measured by Auger electron spectroscopy. Thus, a true bulklike nitride did not form, thereby avoiding complicating issues of vacancy injection from the interface of a growing nitride on silicon.[9]

Isotope profiles were measured *ex situ* with a dual-beam CAMECA IMS-5f SIMS instrument. Sputtering was accomplished with Cs^+ at 2 keV and 60 nA, while analysis was accomplished with Au^+ at 22 keV and 600 pA. The ^{30}Si signal was converted to concentration using the raw ^{28}Si signal together with the known concentration of this latter isotope.

B. Data analysis

The SIMS profiles were analyzed by maximum-likelihood (ML) estimation to determine the surface annihilation probability S. ML estimation finds widespread use in applications such as heat and mass transfer,[10–12] batch crystallization,[13,14] and biological reaction engineering,[15] but has been less commonly used in condensed-matter physics—perhaps because least-squares estimation offers a simpler and more intuitive approach for analyzing systems with few unknown parameters and simple uncertainty structures.

ML estimation proves especially useful for quantifying errors in rate parameters extracted from data sets that have complicated error structures and are described by models incorporating numerous elementary kinetic steps.[16,17] For example, the shapes of the diffusion profiles in the present work are determined by SIMS, which has errors that can vary with both depth and concentration in the specimen. Also, the profile shapes depend upon diffusion of interstitial atoms, growth and dissociation of numerous types of interstitial clusters, and the interaction of interstitials with the crystal lattice and the surface. ML estimation also yields rigorous estimates for the confidence intervals of the derived parameters. These confidence intervals are particularly important for the improvement of the parameter estimates by maximum *a posteriori* (MAP) estimation.[18]

In the present case, the surface annihilation probability S was the only parameter to be determined, and the concentration of ^{30}Si was the only measured variable. The general equations for ML estimation then simplify to minimizing the following functional Φ with respect to S:[16,17]

$$\Phi(S) = \sum_{i=1}^{N_d} w_i (C_i^{^{30}\mathrm{Si}} - \tilde{C}_i^{^{30}\mathrm{Si}})^2, \tag{1}$$

where $C_i^{^{30}\mathrm{Si}}$ and $\tilde{C}_i^{^{30}\mathrm{Si}}$ are the measured and simulated ^{30}Si concentrations at the ith measuring depth and the corresponding weighting factor w_i for each of the N_d data points equals the inverse of the measurement error variance,

$$w_i = \frac{1}{\sigma_i^2}, \tag{2}$$

where σ_i is the standard deviation at each depth. The standard deviation can be approximated by measurement of n different SIMS profiles on the same specimen, yielding

$$\sigma_i = \frac{1}{n-1} \sqrt{\sum_{j=1}^{n} (C_{i,j} - \hat{C}_i)^2}, \tag{3}$$

where $\hat{C}_i$ is the average concentration over the n measurements for the ith depth.

This approach works well when the error comprises primarily random noise, as is typically the case for SIMS.[19] We found, however, that the present profiles also suffered from apparent systematic biases within 1 nm of the surface. Therefore, those data points were excluded from the analysis. Application of Eq. (3) to the remaining data points indicated that the measurement error depended more directly upon isotope concentration rather than upon depth. The standard deviation on a relative basis (i.e., normalized by concentration) obeyed the following square-root relation:

$$\frac{\sigma_i}{C_i} = k_1 \frac{1}{\sqrt{C_i}} + k_2. \tag{4}$$

Here, k_1 and k_2 denote proportional constants, respectively, equal to 4.4×10^8 and 2.7×10^{-2}. Equation (4) indicates that the relative error decreased with the square root of the signal strength—a common occurrence for detectors limited by shot noise.

C. Optimal experimental design

Since specimen preparation, implantation, and profile measurement required significant time and expense, it proved useful to employ model-based optimal experimental design methods to determine the experimental conditions that would maximize the statistical utility of the data. Such methods[17,20,21] are often employed in connection with maximum-likelihood parameter estimation because of the shared mathematical framework. Optimal design entailed using the model to simulate profile evolution under varying hypothetical experimental conditions of ion fluence, ion energy, annealing temperature, and annealing time. A second functional Ψ was optimized according to the criterion of maximizing the sensitivity of the profile to variations in S. This optimization employed finite-difference approximations to the derivative $\partial \tilde{C} / \partial S$, which quantifies how much the simulated isotope concentration changes with S. The functional took the form

$$\Psi(u;\hat{S}) = \sum_{i=1}^{N_d} w_i \left(\frac{\tilde{C}_{i,S+\Delta S}^{^{30}\mathrm{Si}} - \tilde{C}_{i,S-\Delta S}^{^{30}\mathrm{Si}}}{2\Delta S} \right)^2 \Bigg|_{S=\hat{S}}, \tag{5}$$

where u denotes a vector incorporating the four variables describing implantation and annealing conditions, and $\hat{S}$ represents an initial guess of the surface annihilation probability. In our case, the weighting terms w_i come from Eqs. (2) and (4) above. Note that if experimental design must be determined before any data are taken, the standard deviations needed for Eqs. (2) and (3) can be estimated in a preliminary way from prior unrelated measurements taken on the SIMS instrument.

III. SILICON SELF-DIFFUSION MODEL

In Si implanted to significant levels of interstitial supersaturation, self-diffusion behavior is determined primarily by the interplay between interstitials, the surface, and the reservoirs that render interstitials immobile, i.e., lattice sites and interstitial clusters. The model for these interactions was implemented using the profile simulator FLOOPS 2000 (by Law of the University of Florida and Tasch of the University of Texas/Austin),[22] with key rate expressions and rate parameters modified by our laboratory as described in detail elsewhere.[18,23–25] The simulator solves a set of coupled differential equations for the motion and/or reaction of interstitials, lattice sites, and clusters. Previous work published by this laboratory employed FLOOPS to model diffusion of boron in silicon. For the present work, B–Si clustering and kick-out interactions were replaced with the corresponding $^{30}Si-^{28}Si$ interactions.

For computations focusing on optimal experimental design, initial conditions for the profile shapes just after implantation were obtained using the dual-Pearson model for BF_2 implantation[26] in conjunction with scaling of the projected ion range to SiH_4. For computations to determine S, the required initial conditions were obtained using experimental as-implanted profiles. In both cases, 20% of the implanted atoms were assumed to enter substitutional sites, consistent with the suggestions of Caturla *et al.*[27] and Kobayashi *et al.*[28] for boron. Fortunately, sensitivity analysis showed that the results are largely independent of this assumption. Variation of the substitutional percentage over the range of 10%–30% resulted in profile changes smaller than the measurement error in SIMS. The profile of ^{28}Si in interstitial sites was set using the "+1" model[29] in which the concentration exactly tracks the local concentration of ^{30}Si in substitutional sites. The background level of boron doping was sufficiently low that near-surface electric fields[30–32] could be neglected.

A. Interstitial exchange with the lattice

Unlike interstitial clustering, which has been studied extensively,[33–35] there appears to be no literature regarding the kinetics of interstitial exchange with the lattice. However, this mechanism plays an important role in isotopic self-diffusion by sequestering mobile ^{30}Si atoms in the lattice. The present work assumes a direct kick-out-like exchange, possibly through the geometry of the well-known split interstitial.[36,37] (Note that this exchange should be distinguished from "concerted exchange" between two lattice atoms discussed in some papers.[38,39]) This reaction can be written as

$$^{30}Si_i + {}^{28}Si_1 \underset{k_{out}}{\overset{k_{in}}{\rightleftarrows}} {}^{30}Si_1 + {}^{28}Si_i. \tag{6}$$

The rate parameters for this reaction were obtained in separate experiments to be reported elsewhere.[40] The forward reaction that places the mass 30 isotope into the lattice obeys

$$r_{in} = k_{in}[{}^{28}Si_1][{}^{30}Si_i] = K_{in}[{}^{30}Si_i], \tag{7}$$

where the effective first-order rate constant K_{in} has a preexponential factor of $8\times10^{11}\ s^{-1}$ and an activation energy of 1.02 eV. The reverse reaction that kicks the mass 30 isotope back out of the lattice obeys

$$r_{out} = k_{out}[{}^{30}Si_1][{}^{28}Si_i] = K_{out}[{}^{30}Si_1], \tag{8}$$

where the second-order rate constant k_{out} has a preexponential factor of $1.2\times10^{-12}\ cm^3/s$ and an activation energy of 1.02 eV.

B. Surface annihilation rate

In the past work,[32] this laboratory formulated the surface annihilation rate of defects in terms of an annihilation probability S. The probability was written as $S=1-f$, where f represents a fraction that scales the surface concentration with respect to the nearby bulk concentration. The surface flux was written as

$$-D\left.\frac{dC}{dx}\right|_{x=0} = -D\frac{SC_{x=\Delta x}}{\Delta x} = k_r C_{x=\Delta x}, \quad \text{where } k_r = \frac{DS}{\Delta x}. \tag{9}$$

This approach suffers from the drawback that the reaction constant k_r depends upon Δx, which can take on any arbitrary value. (In the calculation of the surface flux, however, variations in Δx are compensated by corresponding variations in $C_{x=\Delta x}$.) It would be preferable to place the reaction constant on a more secure physical basis. The following formulation accomplishes this goal.

Consider a plane of diffusing defects situated one hop length away from the surface. The total impinging flux J_{total} to the surface can be written in terms of the hopping rate Γ and the areal concentration C_A of the impinging defects according to

$$J_{total} = \gamma\Gamma C_A, \tag{10}$$

where γ denotes the fraction of defects that hop towards the surface. (Note that the total flux must be used rather than the net flux given by Fick's Law.) For simplicity, we assume that half of the defects hop toward the surface and half toward the underlying bulk, so that $\gamma=0.5$. This assumption neglects surface-induced lattice distortions that might bias the direction of hopping in the vicinity of the surface. However, such biases are virtually impossible to estimate *a priori*, so we have used the simple statistical treatment here. With the additional assumption of unhindered random-walk motion, Γ can be expressed in terms of the diffusivity D and the jump length λ as

$$\Gamma = \frac{6D}{\lambda^2}. \tag{11}$$

In the present case, we set λ equal to the Si nearest-neighbor distance of 2.73 Å. The areal concentration can be related to the volumetric defect concentration C by

$$C_A = C\lambda. \tag{12}$$

The net flux, which equals the surface annihilation rate, equals the product of the total impinging flux and the surface loss probability,

$$-D \left.\frac{dC}{dx}\right|_{x=0} = J_{\text{total}} S = k_r C, \quad \text{where } k_r = \frac{3DS}{\lambda}. \tag{13}$$

The rate constant k_r can be interpreted as a recombination velocity if the gradients near the surface are small. Equation (13) strongly resembles Eq. (9), if a small enough value of Δx is chosen such that $C_{x=0} \approx C_{x=\Delta x}$. If Δx equals the nearest-neighbor distance in silicon lattice, S determined from the two approaches differs by a factor of 3: the product of the numerical coefficient in Eq. (11) and the fraction of hops towards the surface (i.e., $6 \times 0.5 = 3$).

IV. RESULTS AND DISCUSSION

A. Optimal experimental design

In the present work, the objective function Ψ in Eq. (5) was examined over the following ranges for the four variables: ion energy, 1–3 keV; fluence, 10^{13}–10^{15} ions/cm^2; annealing temperature, 500–1100 °C; and annealing time, 3–240 min. Practical constraints imposed by the apparatus or the SIMS technique determined these ranges. Since the optimal experimental conditions can vary with the value of S, the objective function was maximized for a wide range of S between 10^{-8} and 1.

The optimization procedure for Ψ yielded the following results. The sensitivity of the experiments to S increases as the implant energy decreases, but rather weakly. Sensitivity to ion fluence is stronger, and increases as the fluence increases. Both of these trends held true regardless of the value of S. By contrast, the optimal annealing conditions depended upon the magnitude of S. Three regimes are observed, as shown in Fig. 1.

(1) For large S [≈ 1, Fig. 1(a)], the sensitivity of the experiments decreases as T increases, especially above about 800 °C.
(2) For intermediate S [$10^{-6} \leq S \leq 10^{-2}$, Figs. 1(b)–1(d)], the trend reverses; sensitivity increases as T increases.
(3) For very small S [$< 10^{-8}$, Fig. 1(e)], the sensitivity of the experiments is highest at intermediate temperature ($T \approx 800$ °C). Sensitivity decreases much more slowly when T increases from this point than when T decreases.

In all cases, the effect of annealing time matters only at intermediate temperatures between roughly 700 and 900 °C. For large S (regime 1), shorter annealing times improve sensitivity, while for smaller S (regimes 2 and 3), longer annealing times have this effect.

These complicated behaviors show that the interaction of interstitials with the surface, the lattice, and the cluster reservoirs spawns complicated kinetic phenomena that are not easily predicted *a priori*. Examination of the cluster and interstitial populations did offer some insights, however. A key feature of Si clusters is that the dissociation energy trends generally upward with cluster size to a maximum value of 3.7 eV.[23] Hence, higher temperatures promote the dissociation of progressively larger clusters that release progressively more interstitials (of all isotopes). Free interstitials of ^{30}Si are required for the profile spreading needed to measure S. However, the concentration of free interstitials varies in a complicated nonlinear way with time and temperature because the dissociation of large clusters promotes the growth (or at least the diminished shrinkage) of smaller clusters that would otherwise dissociate quickly. Indeed, it is significant that the intermediate temperatures near 800 °C where the most complicated behavior takes place are roughly the regime in which clusters having slightly less than the maximum dissociation energy begin to fall apart. These clusters are large enough to provide many free interstitials to the system, but small enough to increase their dissociation energy by accreting interstitials themselves. Indeed, formal sensitivity analysis of junction depth and dopant activation during the transient-enhanced diffusion of boron indicates that clusters of this size play an unusually large role in determining these properties of the dopant profile.[23]

The surface exerts an effect as well. Generally speaking, larger values of S promote more rapid cluster dissolution by inhibiting interstitials from adding to clusters. Furthermore, the surface interacts with the lattice reservoir in an important way. Larger values of S tend to pull ^{28}Si interstitials out of the bulk preferentially to ^{30}Si interstitials. The vast majority of ^{28}Si interstitials that exchange with the lattice merely produce more ^{28}Si interstitials, so that exchange events do not significantly impede the motion of these interstitials toward the surface. For ^{30}Si interstitials, the vast majority of exchange events sequester the ^{30}Si in the lattice, producing ^{28}Si interstitials. The ^{30}Si must wait to be kicked out of the lattice before it can move once more, so that the motion of ^{30}Si to the surface is impeded. The nonlinearity of this phenomenon can be seen in the simulated plots of Fig. 2. Large values of S deplete the ^{30}Si profiles near the surface, but otherwise largely freeze the profiles. In contrast, smaller values of S permit a great deal of profile spreading deeper into the bulk. The convolution of such depletion and spreading with the weighted sum of Eq. (5) produces effects that cannot be easily predicted *a priori*.

B. Evaluation of *S*

Figure 3 shows the experimental and simulated profiles for implantation with an energy and dose of 1 keV and 10^{15} cm^{-2}, respectively, followed by annealing at 980 °C for 90 min. The surface was treated before implantation by exposure to ammonia at 1×10^{-6} Torr for 5 min at 800 °C, to give a coverage of about one monolayer (ML) as determined by AES. The value of S emerging from the maximum-likelihood analysis was $(7.11 \pm 0.04) \times 10^{-4}$. This 95% confidence region extends less than 1% on either side of the most likely value. We caution, however, that the computation of this confidence interval included only the effect of stochastic measurement noise, not by various possible model biases. Uncertainties in the activation energies or preexponential factors of the model will propagate through into S. Those numbers have been well tested for modeling other implanta-

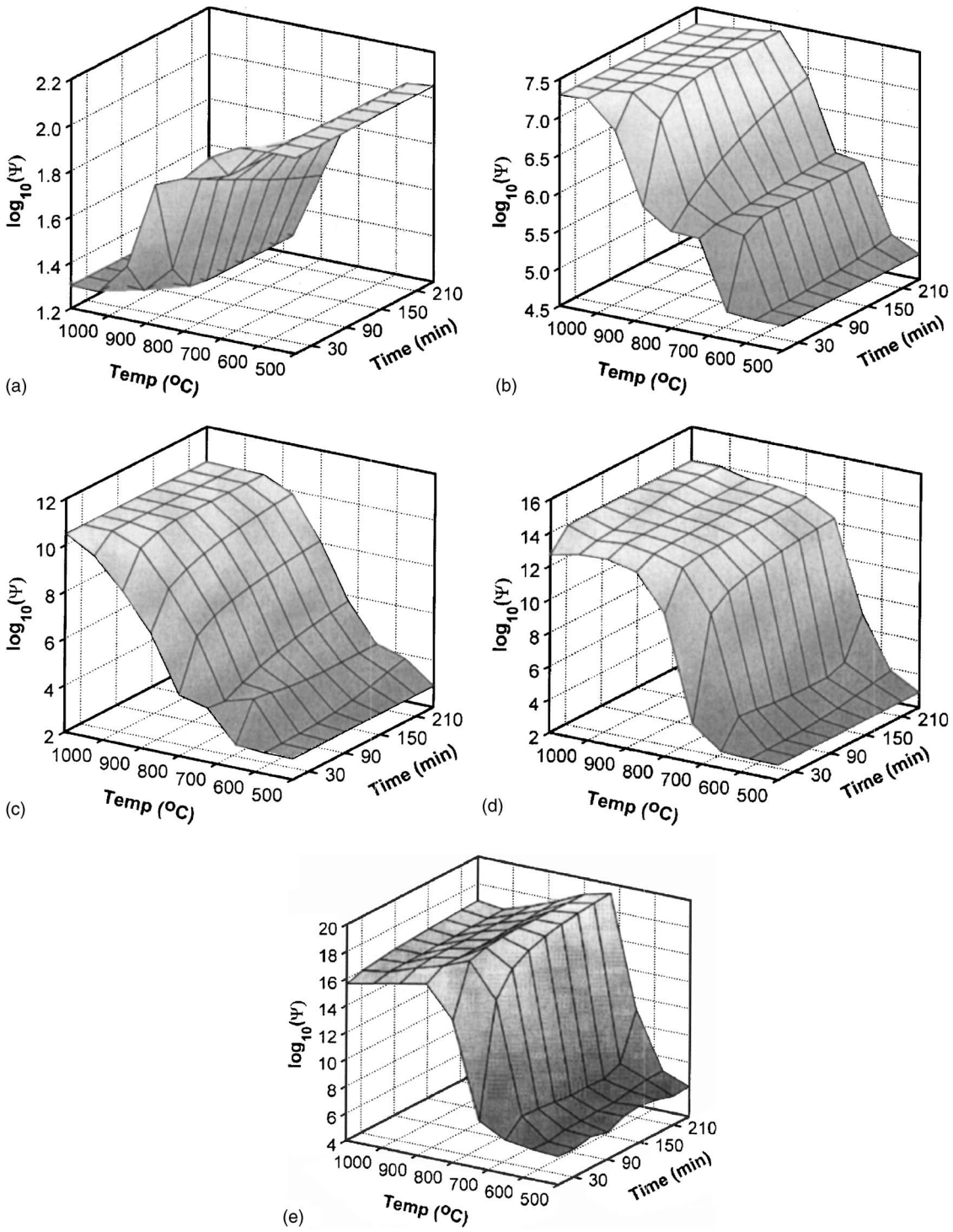

FIG. 1. Plots of the objective function Ψ for optimal experimental design vs annealing temperature for various values of S: (a) 1, (b) 10^{-2} (c) 10^{-4}, (d) 10^{-6}, and (e) 10^{-8}. Implant energy and dose are 1 keV and 10^{15} cm^{-2}, respectively. The larger values of Ψ signify higher experimental sensitivity for measuring S. Sensitivity depends upon the value of S itself, and sometimes varies nonmonotonically with annealing time and/or temperature.

tion systems[18,23–25] (with the exception of the parameters for lattice exchange), but some uncertainties always remain.

The functional form assumed for annihilation represents another possible form of bias. We assumed a constant annihilation probability. However, Vuong *et al.*[41] allowed the interstitial annihilation rate to vary with the number of interstitials trapped at the interface. These workers used the equivalent of a simple Langmuir-like model with $S=S_o(1-\theta)^n$, where θ represents the fractional number of trapping sites filled with interstitials, and n is typically a small integer (0, 1, or 2). Nonzero values of n require a separate mass balance equation for the trapping sites in terms of θ. Reference 41 assumed a value of $n=1$, but gave no value for other parameters that entered into k_r. Such values are nearly impossible to predict *a priori*. In the absence of more knowledge regarding interstitial interactions with interfaces, we have chosen to keep the number of parameters and associated mass balances to a minimum. Thus, we chose $n=0$,

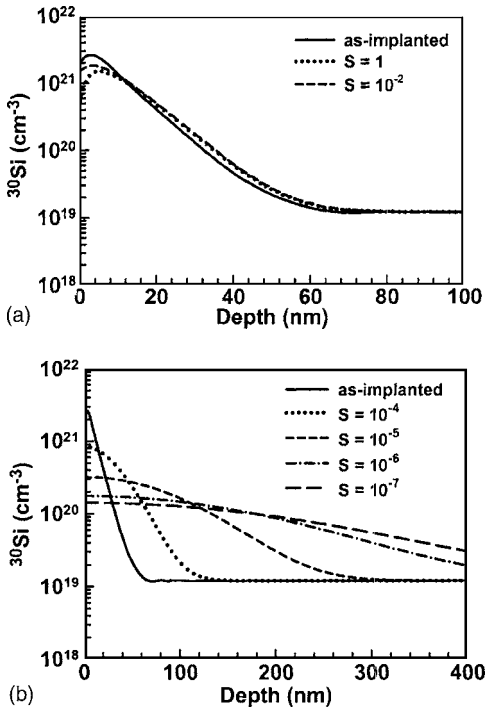

FIG. 2. Simulated ^{30}Si profiles in the regime of (a) high annihilation probability S, and (b) intermediate and low S. Implant energy is 1 keV and dose is 10^{15} cm^{-2}. Annealing temperature and time are 980 °C and 90 min, respectively. Large S induces small amounts of isotope depletion near the surface but greatly inhibits diffusional spreading. Smaller S largely eliminates surface depletion but permits much more spreading.

making S constant. However, the simulated fit to the experimental data is not perfect, which may indicate that another value of n may be more appropriate. A larger body of experimental data will clarify this issue.

The value of S obtained here is rather low—on the order of 10^{-4}. There is little guidance from the literature regarding what value S should take. In particular, there is conflicting evidence concerning the ability of a surface or interface to absorb interstitials of Si, boron, phosphorus, and related elements.[3] Much of the available literature on this subject examines dopant profiles after ion implantation and annealing. During annealing, an interface of Si/SiO_2 typically overlies the diffusing profile. On one hand, experiments have detected a reduction in the size and concentration of {311}

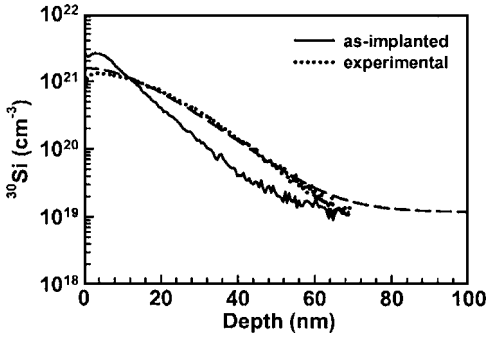

FIG. 3. Experimental and simulated (dashed curve) ^{30}Si profiles. Implant energy and dose were 1 keV and 10^{15} cm^{-2}, respectively, followed by annealing at 980 °C for 90 min. Maximum-likelihood estimation gives $S = (7.11 \pm 0.04) \times 10^{-4}$.

defects with increasing proximity to the interface,[42] suggesting that the interface absorbs Si interstitials fairly efficiently. Some doping profile measurements confirm this suggestion,[43] while other experiments point to a similar conclusion for boron.[42,44] On the other hand, Napolitani *et al.*[45] have cited low levels of boron dose loss compared to phosphorus in order to claim that the interface acts as a poor sink for B_i. Moreover, boron segregates above the solid solubility limit on the Si side of the interface,[46,47] indicating that the interface does not absorb B interstitials very well. This body of work also implies that the interface acts as a poor sink for Si interstitials. Indeed, some laboratories[23,48] have successfully applied a no-flux boundary condition at the interface for both B and Si interstitials. Other workers have avoided discussing the issue altogether by simply not reporting the boundary conditions employed in their models.[46,49]

The experimental work of Voronkov *et al.*[8] also treats annihilation rates of Si interstitials at surfaces, using the spatial distribution of thermal donors in cooled Si wafers as the experimental marker. However, the annihilation rate was assumed to be either zero (under oxygen) or fast enough to yield diffusion-limited interstitial profiles (under vacuum). These approaches do not yield the quantitative values for S that the present method provides. It is clear, however, that the low value of S measured here for a nitrogen-passivated surface is in general agreement with the value of zero assigned to the oxygen-passivated surface in Ref. 8. As shown in Fig. 2(b), however, diffusion profiles in the present experiments continue to change significantly as S decreases from the measured value near 7×10^{-4} down to 10^{-7}. Thus, it is not adequate to assume that the value of S measured here can be approximated by the value of zero.

None of these reports includes a quantitative description of annihilation rates. Description has been at the qualitative level of "efficient" or "poor." The method presented here should offer considerable help in rectifying this gap in quantitative modeling of defect-surface interactions.

V. CONCLUSION

The work develops a method for measuring the surface annihilation probability of point defects. In the case of Si interstitials interacting with N-covered Si(100), the probability is on the order of 7×10^{-4}. Note that the method works for dopants or other foreign species whose diffusion is mediated by interstitials or vacancies. The primary requirement for implementation of the method is a reliable model that describes the interaction of the SIMS-visible species with the mediating defect. It will be interesting to determine whether S varies with crystallographic orientation, degree of adsorption, and other factors.

ACKNOWLEDGMENTS

This work was partially supported by NSF (CTS 02-03237). SIMS was performed at the Center for Microanalysis of Materials, University of Illinois, which is partially supported by the U.S. Department of Energy under Grant No. DEFG02-96-ER45439. We thank Steve Burdin at Isonics Corp. for overseeing the successful creation of isotopically

labeled specimens. We also thank Joel Ager at Lawrence Berkeley National Laboratories for arranging the supply of isotopically labeled silane.

[1]S. M. Hu, J. Appl. Phys. **45**, 1567 (1974).
[2]M. S. Carroll, J. C. Sturm, and T. Büyüklimanli, Phys. Rev. B **64**, 085316 (2001).
[3]P. M. Fahey, P. B. Griffin, and J. D. Plummer, Rev. Mod. Phys. **61**, 289 (1989).
[4]P. Fahey, G. Barbuscia, M. Moslehi, and R. W. Dutton, Appl. Phys. Lett. **46**, 784 (1985).
[5]S. C. Jain, W. Schoenmaker, R. Lindsay, P. A. Stolk, S. Decoutere, M. Willander, and H. E. Maes, J. Appl. Phys. **91**, 8919 (2002).
[6]M. A. Mendicino and E. G. Seebauer, Surf. Sci. **277**, 89 (1992).
[7]M. A. Mendicino and E. G. Seebauer, J. Electrochem. Soc. **140**, 1786 (1993).
[8]V. V. Voronkov, G. I. Voronkova, A. V. Batunina, R. Falster, V. N. Golovina, A. S. Guliaeva, N. B. Tiurina, and M. G. Milvidski, J. Electrochem. Soc. **147**, 3899 (2000).
[9]S. W. Sun, P. J. Tobin, J. Weihmeir, and E. Reed, J. Electrochem. Soc. **134**, 1799 (1987).
[10]T. D. Fadale, A. V. Nenarokomov, and A. F. Emery, Int. J. Heat Mass Transfer **38**, 511 (1995).
[11]Z. M. Cheng and W. K. Yuan, Comput. Chem. Eng. **21**, 511 (1996).
[12]A. Bardow, W. Marquardt, V. Göke, H. Koss, and K. Lucas, AIChE J. **49**, 323 (2003).
[13]S. H. Chung, D. L. Ma, and R. D. Braatz, Chemom. Intell. Lab. Syst. **50**, 83 (2000).
[14]S. M. Miller and J. B. Rawlings, AIChE J. **40**, 1312 (1994).
[15]Ph. Bogaerts, J.-L. Delcoux, and R. Hanus, Chem. Eng. Sci. **58**, 1545 (2003).
[16]I. J. Myung, J. Math. Psychol. **47**, 90 (2003).
[17]J. V. Beck and K. J. Arnold, *Parameter Estimation in Engineering and Science* (Wiley, New York, 1977).
[18]R. Gunawan, M. Y. L. Jung, E. G. Seebauer, and R. D. Braatz, AIChE J. **49**, 2114 (2003).
[19]H. W. Werner, Surf. Interface Anal. **35**, 859 (2003).
[20]E. Walter and L. Pronzato, Automatica **26**, 195 (1990).
[21]P. F. de Aguiar, B. Bourguignon, M. S. Khots, D. L. Massart, and R. Phan-Than-Luu, Chemom. Intell. Lab. Syst. **30**, 199 (1995).
[22]See Mark law, http://www.swamp.tec.ufl.edu/
[23]R. Gunawan, M. Y. L. Jung, R. D. Braatz, and E. G. Seebauer, J. Electrochem. Soc. **150**, G758 (2003).
[24]M. Y. L. Jung, R. Gunawan, R. D. Braatz, and E. G. Seebauer, AIChE J. **50**, 3248 (2004).
[25]M. Y. L. Jung, R. Gunawan, R. D. Braatz, and E. G. Seebauer, J. Electrochem. Soc. **150**, G838 (2003).
[26]A. Tasch, H. Shin, C. Park, J. Alvis, and S. Novak, J. Electrochem. Soc. **136**, 810 (1989).
[27]M. J. Caturla, M. Foad, and T. D. de la Rubia, *International Conference on Ion Implantation Technology*, Kyoto, Japan, 1998 (IEEE, Piscataway, NJ, 1999), Vol. 2, p. 1018.
[28]H. Kobayashi, I. Nomachi, S. Kusanagi, and F. Nishiyama, Mater. Res. Soc. Symp. Proc. **669**, J5.3 (2001).
[29]M. D. Giles, J. Electrochem. Soc. **138**, 1160 (1991).
[30]K. Dev, M. Y. L. Jung, R. Gunawan, R. D. Braatz, and E. G. Seebauer, Phys. Rev. B **68**, 195311 (2003).
[31]K. Dev and E. G. Seebauer, Surf. Sci. **550**, 185 (2004).
[32]M. Y. L. Jung, R. Gunawan, R. D. Braatz, and E. G. Seebauer, J. Appl. Phys. **95**, 1134 (2004).
[33]N. E. B. Cowern *et al.*, Mater. Sci. Semicond. Process. **2**, 369 (1999).
[34]M. P. Chichkine, M. M. De Souza, and E. M. Sankara Narayanan, Phys. Rev. Lett. **88**, 085501 (2002).
[35]A. Claverie, B. Colombeau, G. B. Assayag, C. Bonafos, F. Cristiano, M. Omri, and B. Mauduit, Mater. Sci. Semicond. Process. **3**, 269 (2000).
[36]S. J. Clark and G. J. Ackland, Phys. Rev. B **56**, 47 (1997).
[37]T. Sinno, Z. Kurt Jiang, and R. A. Brown, Appl. Phys. Lett. **68**, 3028 (1996).
[38]K. C. Pandey and E. Kaxiras, Phys. Rev. Lett. **66**, 915 (1990).
[39]P. E. Blöchl, E. Smargiassi, R. Car, D. B. Laks, W. Andreoni, and S. T. Pantelides, Phys. Rev. Lett. **70**, 2435 (1993).
[40]R. Vaidyanathan, M. Y. L. Jung, R. B. Braatz, and E. G. Seebauer, Appl. Phys. Lett. (submitted).
[41]H.-H. Vuong, C. S. Rafferty, S. A. Eshraghi, J. Ning, J. R. McMacken, S. Chaudhry, J. McKinley, and F. A. Stevie, J. Vac. Sci. Technol. B **18**, 428 (2000).
[42]A. Agarwal, H.-J. Gossman, D. J. Eaglesham, L. Pelaz, D. C. Jacobson, T. E. Haynes, and Yu. E. Erokhin, Appl. Phys. Lett. **71**, 3141 (1997).
[43]N. E. B. Cowern, D. Alquier, M. Omri, A. Claverie, and A. Nejim, Nucl. Instrum. Methods Phys. Res. B **148**, 257 (1999).
[44]R. B. Fair, IEEE Electron Device Lett. **20**, 466 (1999).
[45]E. Napolitani, A. Carnera, E. Schroer, V. Privitera, F. Priolo, and S. Moffatt, Appl. Phys. Lett. **75**, 1869 (1999).
[46]A. Shima, T. Jinbo, N. Natsuaki, J. Ushio, J.-H. Oh, K. Ono, and M. Oshima, J. Appl. Phys. **89**, 3458 (2001).
[47]S. Solmi, F. Baruffaldi, and R. Canteri, J. Appl. Phys. **69**, 2135 (1999).
[48]G. Mannino, S. Whelan, E. Schroer, V. Privitera, P. Leveque, B. G. Svensson, and E. Napolitani, J. Appl. Phys. **89**, 5381 (2001).
[49]M. Uematsu, J. Appl. Phys. **84**, 4781 (1998), and references therein.